ACADEMIC PRESS

Available online at www.sciencedirect.com
SCIENCE DIRECT®

Journal of Catalysis 217 (2003) 186–194

JOURNAL OF CATALYSIS

www.elsevier.com/locate/jcat

The nature of cobalt species in Co and PtCoZSM5 used for the SCR of NO_x with CH_4

A. Boix,[a] E.E. Miró,[a] E.A. Lombardo,[a,*] M.A. Bañares,[b] R. Mariscal,[b] and J.L.G. Fierro [b]

[a] *Instituto de Investigaciones en Catálisis y Petroquímica, INCAPE(FIQ,UNL-CONICET), Santiago del Estero 2829, 3000 Santa Fe, Argentina*
[b] *Instituto de Catálisis y Petroleoquímica, Cantoblanco, Madrid, Spain*

Received 16 October 2002; revised 27 December 2002; accepted 3 February 2003

Abstract

A thorough characterization of CoZSM5 and PtCoZSM5 before and after catalytic use was carried out using a battery of techniques. The bimetallic solid was more selective for N_2 production. The TPR profiles showed significant differences. No solid, either fresh or used, exhibited any of the characteristic cobalt oxide X-ray reflections. The XPS data provided information concerning cobalt dispersion. The Raman spectroscopy clearly indicated that Co_3O_4 species were present only in the monometallic zeolites while a form of highly dispersed Co_xO_y moieties became dominant in the PtCoZSM5. The diffuse reflectance spectroscopy showed that Co^{2+} species in the monometallic solids were preferentially located at the main channels while in PtCoZSM5 these cations moved to higher coordination lattice sites. Through the combination of these tools, a much better understanding of the synergetic effect of Pt incorporated to CoZSM5 has been achieved. In view of these findings, related work previously published is revisited.

Keywords: PtCoZSM5; SCR; CH_4; Cobalt species; TPR-Raman

1. Introduction

The allowed levels of NO_x emission from stationary sources are being reduced worldwide [1]. Ammonia-SCR is the proven technology applied to large sources such as power plants. However, no suitable NO_x catalytic reduction method is available for small to medium-scale sources such as cogeneration plants and natural gas-operated engines. In these cases, the use of ammonia becomes economically impractical. This is why the use of natural gas and other related hydrocarbons as reductants is being tried, albeit without much success so far.

M-zeolites (M = Ga, In, Co) are active and selective catalysts for the SCR of NO_x with methane under dry conditions. However, a key factor that has limited their use is the deleterious effect of water upon the selectivity to N_2 production. This effect is particularly evident when methane is used as reductant [2]. Water negatively affects both NO to NO_2 oxidation and NO_2 adsorption, which are known to be fundamental steps of the reaction mechanism [3].

In order to develop more active and stable formulations under the presence of water, the cooperation effect of catalytic species has recently been studied [4]. Kikuchi and co-workers [5,6] performed several studies on the effect of the addition of precious metals (Pt, Rh, and Ir) to In-HZSM5. They reported that such solids are highly selective for the reduction of NO with methane in feed streams containing up to 10% of water, and suggested that the bifunctional feature of such solids is remarkably enhanced by the coexistence of the active sites in the pore of the zeolite, that they call "intrapore catalysis." The same authors [7] and Montes and co-workers [8] found a similar effect in PdCo-containing zeolites. In the same vein, in our group we worked with PtCo mordenites, ZSM5, and ferrierites [9–11]. In most cases, we found that the addition of the noble metal increases the resistance to water deactivation and we concluded that there is a Pt–Co synergism which improves the activity and water resistance, if compared to those of Co monometallic catalysts [9]. We also showed that in order to obtain the desired results a close interaction between Co and Pt is needed. Calcination and/or reduction treatments lead to preferential platinum expulsion from the zeolite lattice and the consequent drop in selectivity. The most selective

* Corresponding author.
E-mail address: nfisico@fiqus.unl.edu.ar (E.A. Lombardo).

0021-9517/03/$ – see front matter
doi:10.1016/S0021-9517(03)00056-3

catalysts contain Co^{2+} at exchange positions plus small clusters of cobalt and platinum oxides. These conclusions were derived from TPR, XPS, and catalytic results but the nature of the said interaction and of the different Co species present at the catalyst surface was not fully understood at that time.

This work is aimed at elucidating how the incorporation of Pt affects the cobalt behavior in PtCoZSM5 using a battery of techniques such as Raman, UV–vis diffuse reflectance, and XPS spectroscopies. DRIFT spectra of adsorbed NO and NO_2 used as probe molecules were also recorded.

2. Experimental

2.1. Preparation of Co and PtCo ZSM5 catalysts

Catalysts were prepared by ionic exchange starting from NaZSM5 (Air product, lot 7461-10252), unit cell $Na_9(AlO_2)_9(SiO_2)_{87} \cdot 16H_2O$. Monometallic cobalt-exchanged NaZSM5 (CoZSM5) solids were prepared using cobalt acetate solution (0.025 M), with 10 g/1.5 L (zeolite/solution) ratio. The exchange time was 24 h at 80 °C (pH 5–6) and then the solids were filtered, washed, and dried at 120 °C for 8 h. An aliquot of this batch was exchanged with a 5×10^{-4} M solution of $Pt(NH_3)_4(NO_3)_2$ using 10 g of zeolite per liter of solution. This exchange was done at room temperature for 24 h. In this way, catalysts containing 4.9 wt% of Co and 0.5 wt% of Pt (PtCoZSM5) and 4.9 wt% of Co (CoZSM5) were obtained.

2.2. Catalytic measurements

Mono and bimetallic powder catalysts were evaluated in a continuous flow system. Prior to the catalytic evaluation, both samples were calcined, heating at 2 °C/min in O_2 flow up to 350 °C. After calcination, the bimetallic sample was reduced in H_2 at 350 °C. The typical composition of the reacting stream was the following: 1000 ppm NO, 1000 ppm CH_4, 2% O_2, and 2% H_2O in helium. The reaction was performed under atmospheric pressure at temperatures between 350 and 600 °C, with GHSV = 10,000 h^{-1}. The catalysts were kept on stream for a period of 16–20 h. The gaseous mixtures were analyzed with an SRI 9300B chromatograph equipped with two columns, a 5-Å molecular sieve, and a Chromosorb 102. The NO conversion (C_{NO}) was calculated from N_2 production: $C_{NO} = 2 \times 100 \times ([N_2]/[NO]^0)$, where $[NO]^0$ is the NO initial concentration. The CH_4 conversion (C_{CH_4}) was obtained as $C_{CH_4} = 100 \times ([CH_4]^0 - [CH_4])/[CH_4]^0$.

2.3. TPR experiments

These experiments were performed with 50–100 mg of either the calcined or the used catalyst using an Okhura TP-2002 S instrument equipped with a TCD detector. The reducing gas was 5% H_2 in Ar, flowing at 30 mL/min, and the heating rate was 10 °C/min.

2.4. DRIFTS

Diffuse-reflectance infrared spectra were collected on a Nicolet-510 FTIR spectrophotometer working at a resolution of 4 cm^{-1} using a Harrick HVC-DRP environmentally controlled cell. The samples, ca. 30 mg, were placed in the DRIFT cell and pretreated in situ following the same procedures used in Section 2.2. The sample was subsequently cooled to room temperature in He flow prior to exposure to the adsorption mixture, 3000 ppm NO (Ar). Once the spectrum was recorded at room temperature, a He gas stream was fed to the cell to remove the physisorbed species. In this atmosphere the temperature was increased up to 400 °C, heating rate 10 °C/min. The IR single-beam background spectrum of the pretreated solid was recorded at a given temperature, and then subtracted from the single-beam spectrum of the sample obtained at the same temperature. At each temperature, 256 scans of the spectra were collected.

2.5. Surface analysis by XPS

X-ray photoelectron spectra were acquired with an ESCALAB 200R electron spectrometer equipped with a hemispherical electron analyzer and Al-K_α X-ray source ($h\nu$ = 1486.6 eV). The Si 2p, Al 2p–Pt 4f, Pt 4d, Co 2p, O 1s, and C 1s core-level spectra were recorded for all the samples. As the Co 2p and Pt 4d signals were very weak, the corresponding energy regions were scanned 200 times in order to improve the signal-to-noise ratio. All the peaks were fitted by a Gaussian–Lorentzian component waveform after an inelastic (Shirley-type) background had been subtracted. For the Al 2p and Pt 4f peaks, the situation was more complex because they overlapped.

In order to calculate the surface atomic ratio (n_i/n_j) the following equation was used:

$$n_i/n_j = (I_i/I_j)(\sigma_j/\sigma_i)(\mathrm{KE}_i/\mathrm{KE}_j)^{1/2},$$

where I is the intensity of the peak, σ is the ionization cross section, and KE is the kinetic energy of the element i or j, respectively. The samples calcined and the catalysts used in the SCR reaction were dehydrated in vacuum (10^{-5} Torr), followed by heating at a rate of 5 °C/min up to 350 °C to remove adsorbed water.

2.6. Raman spectroscopy and TPR-Raman

The Raman spectra were run with a Renishaw System-1000 microscope Raman spectrometer with an Ar^+ laser as exciting source at 514 nm. Raman spectra during TPR (TPR-Raman) experiments were run with a hot stage (Linkam TS-1500) that can be heated up to 1500 °C under flowing gases. TP-Raman experiments were run by heating the sample in

steps of 50 °C. Spectra were acquired at each temperature, with a resolution of 2 cm^{-1}. Laser power was 12 mW. A 1% H_2 in Ar (SEO-L'Air Liquide) was used for the TPR-Raman experiments. Selected spectra are presented to illustrate the trends.

2.7. Diffuse reflectance spectroscopy (DRS)

UV–vis spectra were recorded using a UV-2401-PC Shimadzu Spectrometer equipped with a DR attachment with an integrating sphere coated by $BaSO_4$. The spectra were recorded at room temperature in differential mode with NaZSM5 as reference. The absorption intensity was calculated from the Schuster–Kubelka–Munk equation.

3. Results

3.1. Catalytic data and TPR profiles

Table 1 shows the catalytic data and the hydrogen consumption of the calcined and used solids. As previously shown in greater detail for mordenite, ferrierite, and ZSM5, the incorporation of Pt to Co zeolites increases both the selectivity to N_2 and the resistance to water inhibition [10].

Fig. 1 shows the TPR profiles of both the calcined and the used CoZSM5 solid. After use, two main differences are noted. On the one hand, while in the used catalyst the cobalt is 90% reduced, only ca. 50% is reduced in the calcined solid (Table 1). On the other, the reduction temperatures of the three distinguishable peaks significantly decrease.

Fig. 2 shows the TPR profiles of the PtCoZSM5 solid. The presence of Pt promotes the cobalt reduction, decreasing the peak temperatures and increasing the H_2 consumed in the calcined solid (Table 1). In this case, both the calcined and the used solid are incompletely reduced, roughly 75% of the cobalt (Table 1). Note that the calcined catalyst exhibits two peaks, a small one at 210 °C and the other at 590 °C (Fig. 2a) while the used catalyst exhibits three peaks at 210, 300, and 600 °C. The peak at 210 includes the Pt^{2+} reduction (Table 1). It seems that after use, the peak at 590 °C splits in two, centered at 300 and 600 °C. Or, maybe, there are two peaks under the high temperature trace.

At this point, it was thought that NO adsorption monitored by FTIR could show the existence of different adsorption sites in the solids before and after use.

Table 1
Catalytic data and H_2 consumption measured in the TPR experiments

Catalysts	% Conversion[a]			TPR data: H_2/Co,[b] T_{max} (°C)		
	NO	CH_4	Treatment	Peak 1[c]	Peak 2[c]	Peak 3[c]
CoZSM5	17.0	65.0	Calcined	–	0.1 (450)	0.38 (710)
			Used	0.08 (270)		0.82 (595)
PtCoZSM5	22.7	74.7	Calcined	0.06 (210)[d]	–	0.62 (590)
			Used	0.03 (210)[d]	0.34 (300)	0.38 (600)

[a] Reaction conditions: GHSV = 10,000 h^{-1}, temperature 500 °C, 1000 ppm NO, 1000 ppm CH_4, 2% O_2 and 2% H_2O.
[b] µmol of H_2/µmol of Co.
[c] Peak temperatures are given between parentheses.
[d] The H_2 consumption for Pt^{2+} reduction (0.03) has been subtracted.

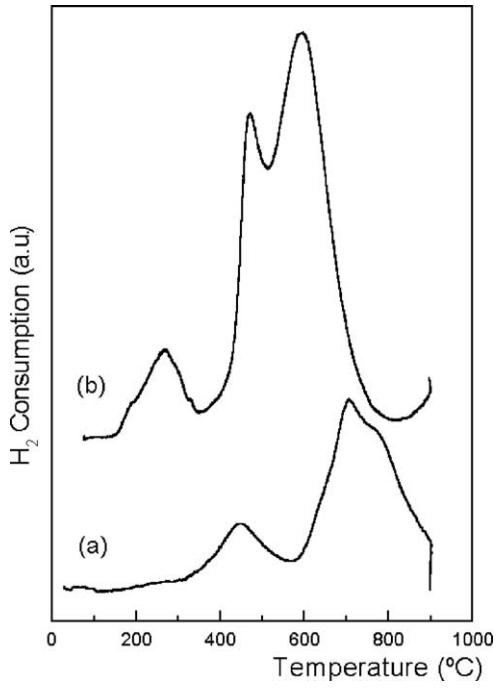

Fig. 1. TPR of CoZSM5. (a) Calcined at 350 °C. (b) After use. Reducing gas 5% H_2/Ar, heating rate 10 °C/min up to 800 °C.

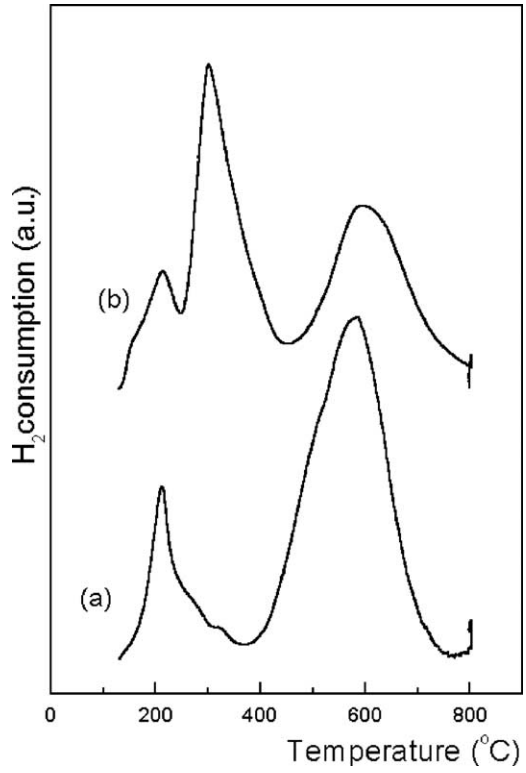

Fig. 2. TPR of PtCoZSM5. (a) Calcined at 350 °C. (b) After use. Reducing gas 5% H_2/Ar, heating rate 10 °C/min.

3.2. DRIFT data

Fig. 3A shows the spectra obtained when NO was adsorbed at 22 °C on calcined CoZSM5 and then desorbed at increasing temperatures till 400 °C. The two bands at 1811 and 1895 cm^{-1} are assigned to the dinitrosyl adsorbed on exchanged Co^{2+} cations. The appearance of a third band at 1850 cm^{-1} after desorption at 350 °C is likely due to the decomposition of the dimer, as reported by Ivanova et al. [12].

The same spectra were obtained with both the used monometallic and the calcined PtCoZSM5 solid. Fig. 3B shows the spectra obtained when NO was adsorbed on used PtCoZSM5. The dimer bands appear at the same frequencies but in this case, the 1850 cm^{-1} signal was not observed. In separate experiments, NO_2 was also adsorbed on the four solids but again no significant differences were observed among the recorded spectra.

Could a surface technique show changes in binding energies of the cations and/or surface atomic ratios symptomatic of surface processes occurred during the catalytic act?

3.3. XPS data

Table 2 shows the data obtained with the four solids. First note that there is no significant difference in Co 2p BEs for all the samples, except for a small decrease in the bimetallic sample after use. The BE values are located somewhere in between Co^{2+} at exchange positions (∼782 eV) and Co^{n+} in cobalt oxides, ca. 780 eV [13,14]. Note that Co^0 BE is ca. 778 eV. Si 2p and Al 2p peaks exhibit BE values expected for the zeolites. Platinum, first located at exchange positions and hardly visible, seems to be partially reduced after reaction. Remember that the fresh catalyst has been prereduced at 350 °C to obtain the best catalytic performance. The BE of 317.5 eV is uncertain due to the weakness of the Pt signal in the fresh solid (note the very low Pt/Si ratio).

Another important piece of information emerges from the observation of the Co/Si ratio. This value is significantly higher for the bimetallic zeolite. This might indicate a higher Co dispersion in these solids than in their monometallic counterparts. The monometallic zeolite does not show a

Table 2
XPS data of calcined (fresh) and used catalysts[a]

Sample	Binding energies (eV)				Atomic surface ratio		
	$Co2p_{3/2}$	$Pt4d_{3/2}$	Si2p	Al2p	Pt/Si	Co/Si	Si/Al
CoZSM5							
Calcined	781.7	–	103.1	74.5	–	0.58	10.8
Used	781.1	–	102.8	74.5	–	0.58	13.3
PtCoZSM5							
Calcined	781.3	317.5	102.7	74.2	6×10^{-4}	1.20	10.6
Used	780.9	316.2 (39%) 318.5 (61%)	102.6	74.4	1.3×10^{-2}	0.96	10.8

[a] Al-K_α X-ray source. The samples were heated up at 5 °C/min up to 350 °C in situ before the spectra were taken.

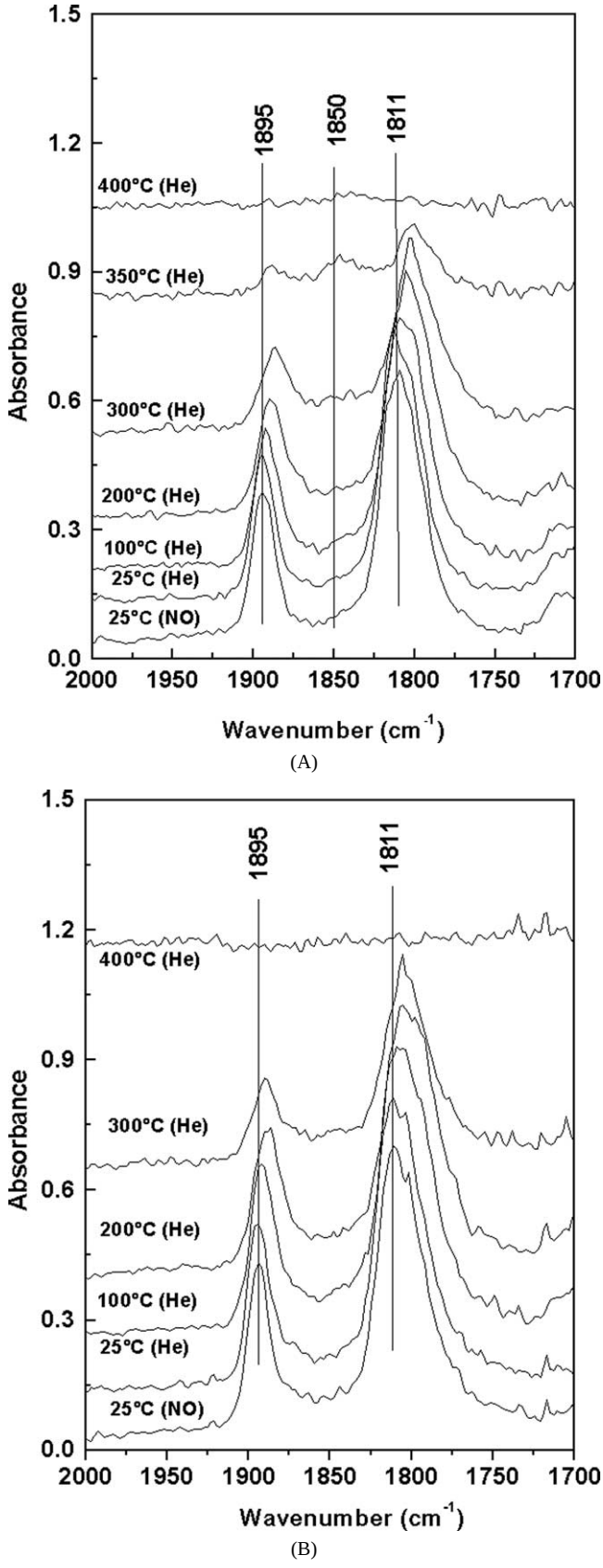

Fig. 3. DRIFT spectra of adsorbed NO on calcined CoZSM5 (A) and used PtCoZSM5 (B). The bottom spectrum was recorded in the presence of NO and the following after flushing with He at increasing temperatures.

significant change in the dispersion of cobalt after its use in the reaction, while the bimetallic zeolite does show a decrease of the exposure of cobalt (Table 2).

3.4. Raman spectroscopy data

Fig. 4 presents the Raman spectra of calcined CoZSM5, used CoZSM5, and NaZSM5 reference. NaZSM5 exhibits a broad Raman band near 370 cm^{-1}. The calcined CoZSM5 exhibits Raman bands near 681, 530, and 485 cm^{-1}, characteristic of the Co_3O_4 phase [1]. The broad Raman band near 598 cm^{-1} is characteristic of dispersed cobalt oxide species [15]. The Raman spectra of used CoZSM5 exhibits sharper Raman bands near 681, 530, and 482 cm^{-1}. The intensity of these bands increases with respect to that of dispersed cobalt Raman band at 598 cm^{-1}. This observation is indicative of a rearrangement from dispersed cobalt oxide to the Co_3O_4 phase. Small Co_3O_4 domains with sizes below 4 nm should be developed since no characteristic reflection of the cobalt oxide is observed in the XRD patterns.

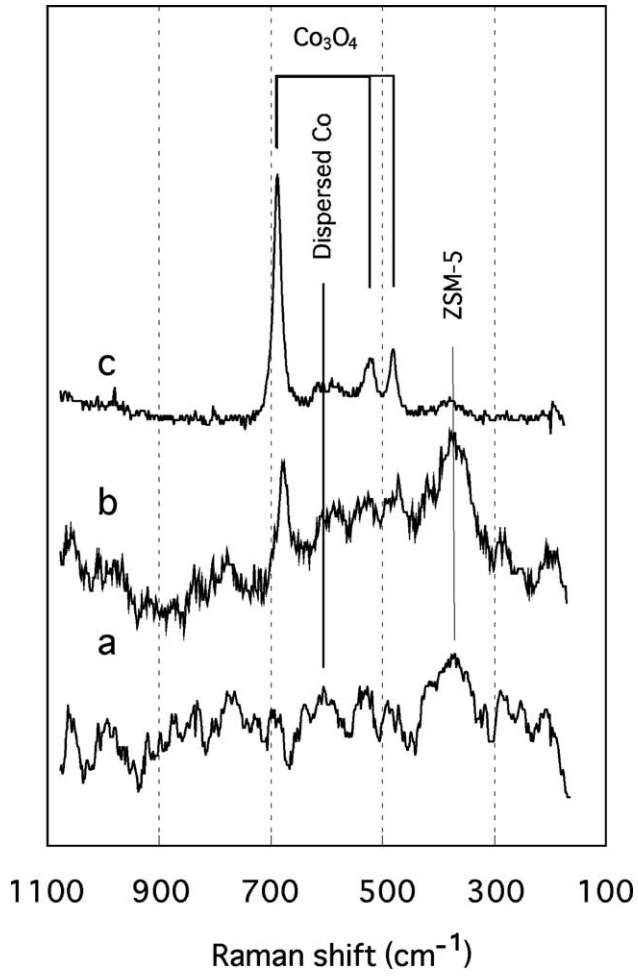

Fig. 4. Laser Raman spectra of cation-exchanged ZSM5 recorded at 22 °C. (a) NaZSM5 calcined at 350 °C; (b) CoZSM5 calcined at 350 °C, and (c) used CoZSM5.

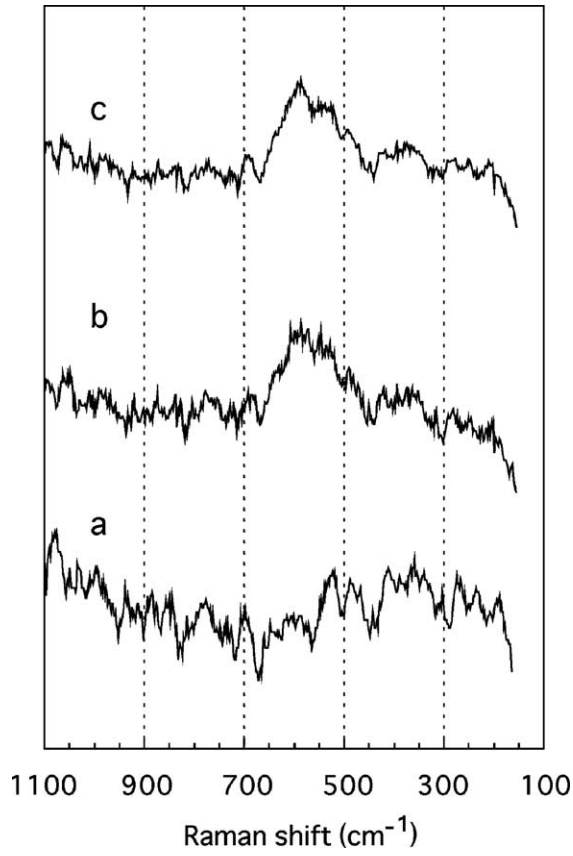

Fig. 5. Laser Raman spectra of PtCoZSM5 calcined at 350 °C: (a) recorded at 22 °C and (b) recorded at 450 °C in He flow and (c) used under reaction conditions.

The fresh PtCoZSM5 catalyst exhibits no Raman features of Co_3O_4 or of dispersed cobalt oxide species (Fig. 5a). Thus, it is likely that Co species are located at exchange positions in the zeolite lattice. During in situ treatment in He at 450 °C, a new Raman band near 598 cm^{-1} becomes apparent (Fig. 5b). This Raman band is characteristic of dispersed cobalt oxide species [15]. Note that the Raman spectra of calcined and used CoZSM5 catalysts (not shown) are not affected by the temperature of the sample during spectral acquisition in the 20–500 °C range.

The Raman spectra of used PtCoZSM5 catalysts also exhibit a new Raman band near 598 cm^{-1} (Fig. 5c), characteristic of dispersed cobalt oxide species. Therefore, in bimetallic zeolites the cobalt species appear to leave exchange sites upon heating or under use in reaction.

Fig. 6 shows representative spectra of the TPR-Raman study of calcined CoZSM5. As the reduction temperature increases, the Raman bands of Co_3O_4, at 681, 530, and 485 cm^{-1}, decrease in intensity, and are almost absent by 500 °C. The Raman band at 598 cm^{-1} appears less affected in this temperature range, but it significantly reduces its intensity by 600 °C. This result indicates reduction of Co_3O_4 at lower temperatures than dispersed cobalt oxide species. The shift to lower temperatures in the TPR profiles of the used catalysts is consistent with an aggregation of

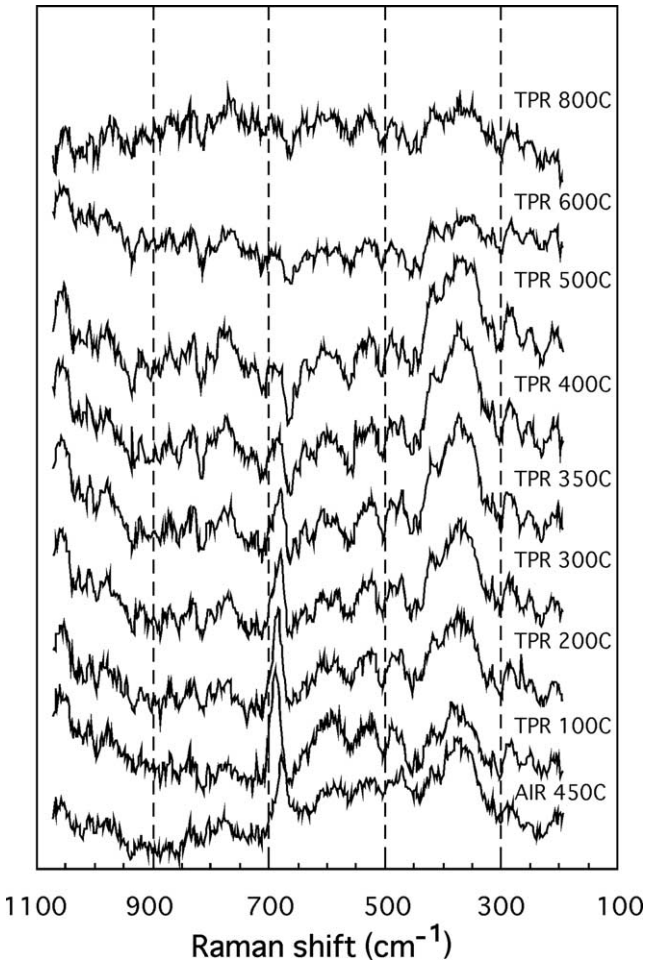

Fig. 6. Laser Raman spectra of CoZSM5 calcined at 350 °C; reduced in situ with 1% H_2 in Ar.

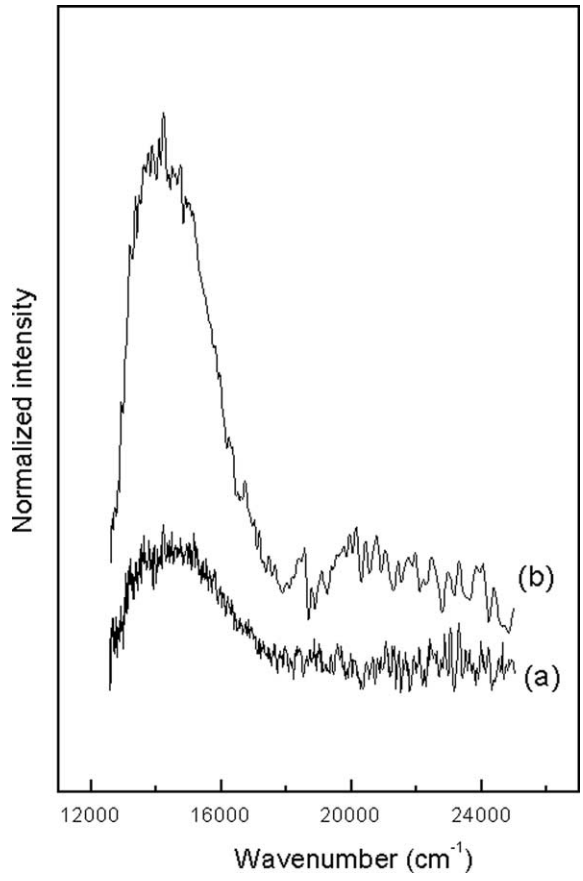

Fig. 7. UV–vis DRS of CoZSM5 (a) calcined at 350 °C (b) after use. Absorption intensity calculated from the Schuster–Kubelka–Munk equations.

dispersed cobalt oxide species into more reducible Co_3O_4 microcrystallites. The relative intensities for the reduction of Co_3O_4 and dispersed cobalt oxide species suggest that there is a larger population of dispersed cobalt oxide species. Thus, it appears that the Raman cross section of microcrystalline Co_3O_4 must be higher than that of dispersed cobalt oxide species.

3.5. UV–vis diffuse reflectance spectroscopy

DRS was used to elucidate whether or not the presence of Pt modifies the location of the Co^{2+}.

Fig. 7 shows the DRS data obtained with both the fresh and the used CoZSM5. Note that in both cases, the signal frequency (ca. 14,500 cm^{-1}) has been assigned to Co^{2+} cations located in the straight channels of the MFI structure: α-sites according to Wichterlová and co-workers [16,17].

Fig. 8 shows the same data for fresh and used PtCoZSM5. One significant difference with Fig. 7 is the appearance of a second larger band at a higher wavenumber. In the case of fresh PtCoZSM5, the second band appears at 19,000 cm^{-1} and is asymmetric. This spectrum seems to indicate that Co^{2+} is now populating better shielded β sites, that the population of α-sites has decreased, and that maybe there is a much smaller number of ions in the highest coordination γ-sites. After use, the Co^{2+} ions seem to have moved from the β to the γ-sites because the second signal is now centered at 23,000 cm^{-1}.

The Co_3O_4 visible in the Raman spectra of CoZSM5 is also detected by DRS in the used catalyst. This oxide exhibits two broad bands at ca. 15,000 and 26,000 cm^{-1} [18]. The former signal may be partially included in the band centered at 14,200 cm^{-1} (Fig. 7b) but the other was present in the spectra (frequency not shown). Due to the lower sensitivity of DRS compared to LRS for the detection of Co_3O_4 6300 cm^{-1} is not seen in the case of calcined CoZSM5.

4. Discussion

When cobalt is exchanged in ZSM5, different species are formed, depending on the exchange procedure and on the pretreatments. Cations at exchange positions, Co_3O_4 crystals, highly dispersed noncrystalline cobalt oxide species, and polynuclear Co oxo-ions, are reported in the literature as the main observable species [16,17,19,20]. Among these, Co at exchange positions are responsible for the activity in

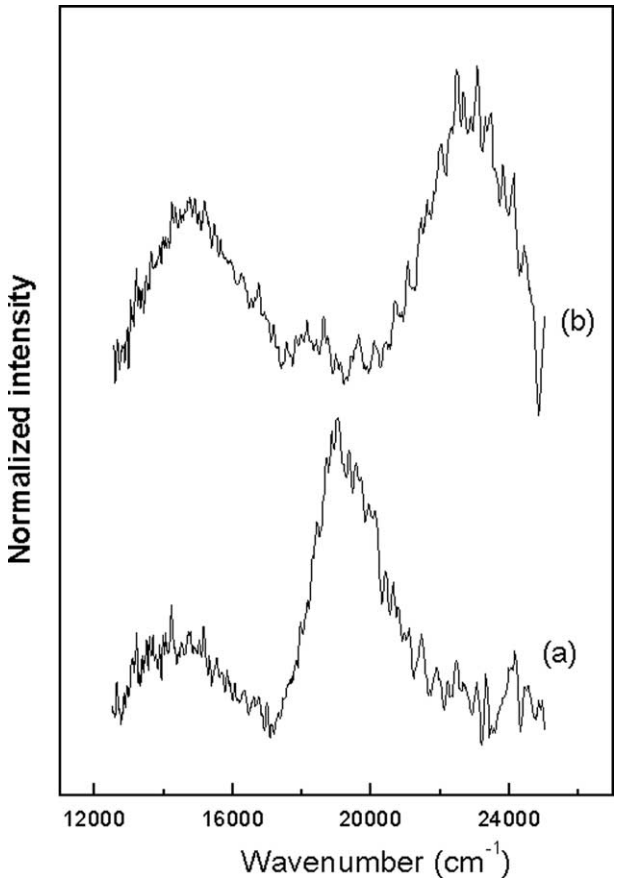

Fig. 8. UV–vis DRS of Pt/CoZSM5 (a) calcined at 350 °C (b) after use. Absorption intensity calculated from the Schuster–Kubelka–Munk equations.

the SCR of NO_x with methane [17,22]. The pentasil structure of ZSM5 offers three different sites to Co exchange: the α-type site is suggested to be coordinated to four oxygen atoms of the straight channel wall, the β-site is located at the distorted six-member ring at the intersection of straight and sinusoidal channels, and the γ-site is located at the sinusoidal channel (boat-shaped sites) [17]. On the other hand, Co_3O_4 is a nondesired species because it only promotes the methane oxidation with oxygen instead of NO_2.

The calcined cobalt-exchanged ZSM5 exhibits the Raman bands of Co_3O_4. This oxide could be formed by dehydration of cobalt hydroxide precipitated inside the zeolite channels. Schoonheydt et al. [21] studied the exchange of Cu^{2+} and Ni^{2+} in X and Y zeolites at pH 5–7 and suggested the presence of $M_x(OH)_y{}^{(2x-y)+}$ complexes in solution. These complexes may either be exchanged or precipitate inside or on the surface of the aluminosilicate. A similar mechanism may be operative when cobalt acetate is used. In any case, the fraction of precipitated cobalt hydroxide is about 10% of the total cobalt.

After reaction, the Co_3O_4 Raman triplet clearly dominates the spectrum (Fig. 4). The intense Raman bands of Co_3O_4 might suggest that the Co 2p BE should move toward the 780–781 eV range. The XPS data do not show such a trend (Table 2). However, it should be noted that Raman spectroscopy cannot provide information about the Co^{2+} species at exchange positions and that the Raman cross section of microcrystalline Co_3O_4 must be rather high.

The incorporation of platinum inhibits the formation of Co_3O_4. Instead, a highly dispersed Co_xO_y species develops after heating the sample in He at 450 °C (Fig. 5). The exposure to the reactant stream does not modify the spectra (compare spectra a and b in Fig. 5).

The incorporation of platinum induces a different behavior of the cobalt cations. The adsorption of both NO and NO_2 on these catalysts does not yield any additional information concerning this matter. The XPS data evidence a higher degree of dispersion in the bimetallic solid since the Co/Si atomic ratio for the PtCoZSM5 is twice that of CoZSM5 (Table 2). This is consistent with the Raman results. Note that the used PtCo catalyst only displays the signal corresponding to highly dispersed Co_xO_y (Fig. 5, c) while the used CoZSM5 shows the presence of Co_3O_4 (Fig. 4, c).

A clearer picture is obtained from the DRS spectra. The CoZSM5 catalyst contains, almost exclusively, Co^{2+} ions in the α position (Fig. 7). However, when Pt is incorporated the Co^{2+} cations move to more shielded positions with higher coordination numbers. This effect becomes more evident after exposure to the reactant stream (Fig. 8). It seems then that the incorporation of platinum displaces the Co^{2+} cations to locations inside the lattice. These cations are now harder to extract from the lattice and no Co_3O_4 is detected by any of the techniques used. The Raman spectra particularly support this finding.

The behavior of the monometallic solid may suggest that after use, a significant portion of the cations have left the exchange positions to form a cobalt oxide phase. Raman spectroscopy shows that a fraction of this cobalt is present as dispersed oxide and another as microcrystalline Co_3O_4, neither of them detectable by XRD, so the oxide phase must be smaller than 4 nm. Therefore, cobalt species appear to leave the zeolite lattice during use in reaction. Cobalt is more dispersed on PtCoZSM5. The TPR profiles suggest that the dispersion of cobalt is worse on CoZSM5 than on PtCoZSM5 and that both catalysts decrease the exposure of cobalt after use in the reaction. Both trends are consistent with the Raman results.

The TPR data are consistent with this overall picture. It is well known that the calcined CoZSM5 is difficult to reduce [22]. Only 50% of the Co^{2+} can be reduced. After reaction, however, when sharp Co_3O_4 bands dominate the Raman spectra, almost 90% of the cobalt ions are reduced to Co^0 (Table 1). Furthermore, in this case the cations are mostly located at exchange positions with the lowest oxygen coordination (weaker bonding to the lattice). In line with this, DRIFT spectra (Fig. 3) show the adsorption of dinitrosyl species whose formation is favored on α-sites [17].

When Pt is present, two opposing phenomena occur:

(i) The presence of Pt facilitates the reduction of cobalt either exchanged or in a highly dispersed form. This is reflected in lowering the temperatures at which the two reduction peaks appear in the calcined solids (compare Figs. 1a and 2a).
(ii) The used PtCoZSM5 is less reduced than the used CoZSM5 (Table 1). This is also consistent with the fact that most of the exchanged Co^{2+} cation has moved to better shielded lattice sites (Fig. 8).

The in situ TPR-Raman studies (Fig. 6) demonstrate that the reduction of Co_3O_4 occurs at a lower temperature than that of the highly dispersed cobalt oxide. Thus, the reduction peak centered at 450 °C (Fig. 1a) includes both Co_3O_4 and dispersed oxide. After use, this peak has split in two (Fig. 1b). The first one at 270 °C corresponds to Co_3O_4 while the second peak at 470 °C should represent the reduction of the dispersed oxide.

With regard to the role of the different Co species on the SCR of NO_x with methane, it has been proposed that Co^{2+} at exchange sites are mainly responsible for the activity and selectivity toward nitrogen. It has been suggested that β-type cobalt ions, coordinated to the distorted six-membered ring of the ZSM5 framework at the intersection of straight and sinusoidal channels, possess the highest activity [17]. Coincidentally, we have found that Pt displaces the Co^{2+} cations from the α position to locations inside the lattice, and this is consistent with the observed increase in the activity. Thus, not only is the beneficial effect of Pt addition related to its intrinsic activity to oxidize NO and to adsorb NO_2, but it also ameliorates the cobalt role in the reaction mechanism.

The question has been raised as to whether the Co^{2+} migration to higher coordination sites could be achieved through heat treatment. We have wash-coated CoZSM5 to cordierite monoliths calcining the system at 550 °C [23]. This monolith showed, however, the same catalytic behavior as the CoZSM5 in powder form, calcined at 350 °C.

As said before, it is known that the presence of Co_3O_4 is detrimental for the N_2 selectivity of this reaction. The question now is, what is the role (if any) of the highly dispersed Co_xO_y species? We have previously reported [9,10] that neither a mechanical mixture of Pt and Co zeolites nor two bed arrangements lead to enhanced N_2 production. Thus, a close Pt–Co interaction is needed to improve catalytic performance. It is probable that these Co moieties can interact more easily with Pt due to its high dispersion.

All the positions for cobalt exchange are accessible to reactants, the α position being the one with the lowest coordination. However, Kaucký et al. [17] suggested that for the activity of Co ions, not only might the expected strength of bonding of the Co ions to the framework be important but also the cation location in the inner volume of the zeolite. Inside the MFI structure the β-sites are the most advantageous for reactant adsorption and intermediate formation. It is also suggested that the distance between Co ions and other sites in which NO oxidation takes place is important. The active sites may be two cobalt ions, a Co ion with a proton, or a Co ion with Co_xO_y species. Our results suggest that Pt–Co clusters (the latter in the form of Co_xO_y) are responsible for NO oxidation and NO_2 adsorption, methane being activated in either the α or β neighboring Co cations. In line with this idea, TPR data show that reduction peaks of both oxide and exchanged Co species are shifted to lower temperatures, indicating the intimate interactions of Pt with Co_xO_y and Co^{2+} at α and/or β positions.

5. Conclusions

Through this study, we have been able to clearly identify the cobalt species present in Co and PtCoZSM5 calcined at 350 °C as well as the changes occurring in them after use in the SCR of NO_x with CH_4.

After calcination, the monometallic CoZSM5 catalyst contains Co_3O_4, Co_xO_y, and Co^{2+} located at exchange positions (Fig. 4b). After exposure to the reactant stream containing 2% water, the Co_3O_4 becomes dominant (Fig. 4c). This evolution is also confirmed by the H_2 consumption data (Table 1). The Co_3O_4 is not detected in the XRD patterns. The DRS spectra show that the Co^{2+} are mainly located at the main ZSM5 channels (Fig. 7) and do not migrate to better shielded lattice positions.

The bimetallic PtCoZSM5 formulation calcined at 350 °C only contains Co^{2+} (Fig. 2a and Table 1). The location of the Co^{2+} ions has changed by the introduction of platinum. In the calcined catalyst, a large fraction of the ions has migrated to internal lattice positions (Fig. 8a). After use (Fig. 8b), the ions migrate to the highest coordinated sites (γ). This catalyst contains both Co^{2+} at exchange positions and highly dispersed cobalt oxide (Fig. 5c).

All these results are consistent with the improved performance of the bimetallic formulations (see Table 1 and Refs. [9,10]). In CoZSM5, the presence of Co_3O_4, a good methane oxidation catalyst, deleteriously affects the N_2 selectivity. With the introduction of Pt, the Co^{2+} migrates to harder-to-reduce exchange positions and Co_3O_4 is not formed.

Acknowledgments

The authors acknowledge the financial support received from UNL, CONICET, and ANPCyT. Thanks are also given to the Spanish International Cooperation Agency, and to the CYTED Program for financing the mobility between groups. CICYT Grant IN96-0053, Spain, partially funded the acquisition of the Raman spectrometer. The authors also appreciate the donation of the major instruments from the Japan International Cooperation Agency (JICA), and Elsa Grimaldi's edition of the English manuscript.

References

[1] H. Ohtuska, T. Tabata, O. Okada, L.M.F. Sabatino, G. Bellussi, Catal. Lett. 44 (1997) 265.
[2] J. Armor, Catal. Today 26 (1995) 147.
[3] M. Ogura, M. Hayashi, E. Kikuchi, Catal. Today 42 (1998) 159.
[4] H. Hamada, Catal. Surv. Jpn. 1 (1997) 53.
[5] E. Kikuchi, M. Ogura, N. Aratani, Y. Sugiura, Hiramoto, K. Yogo, Catal. Today 27 (1996) 35.
[6] M. Ogura, M. Hayashi, E. Kikuchi, Catal. Today 42 (1998) 159.
[7] M. Ogura, Y. Sugiura, M. Hayashi, E. Kikuchi, Catal. Lett. 42 (1996) 185.
[8] F. Bustamante, F. Córdoba, M. Yates, C. Montes, Appl. Catal. A Gen. 234 (2002) 127.
[9] L. Gutierrez, A. Boix, E. Lombardo, J. Fierro, J. Catal. 199 (2001) 72.
[10] L. Gutierrez, A. Boix, J. Petunchi, Catal. Today 54 (1999) 451.
[11] L. Gutierrez, A. Boix, J. Petunchi, J. Catal. 179 (1998) 179.
[12] E. Ivanova, K. Hadjiivanov, D. Klissurski, M. Bevilacqua, T. Armaroli, G. Busca, Micropor. Mesopor. Mater. 46 (2001) 299.
[13] Z. Zsoldos, G. Vass, G. Lu, L. Guczi, Appl. Surf. Sci. 78 (1994) 467.
[14] A. Boix, J.L.G. Fierro, Surf. Interface Anal. 27 (1999) 1107.
[15] M. Vuurman, D. Stufkens, A. Oskam, G. Deo, I. Wachs, J. Chem. Soc., Faraday Trans. 92 (1996) 3259.
[16] J. Dedecek, D. Kaucký, B. Wichterlová, Micropor. Mesopor. Mater. 35–36 (2000) 483.
[17] D. Kaucký, A. Vondrová, J. Dedecek, B. Wichterlová, J. Catal. 194 (2000) 318.
[18] J. Yan, M.C. Kung, W.M.H. Sachtler, H.H. Kung, J. Catal. 172 (1997) 178.
[19] X. Wang, H. Chen, W.M.H. Sachtler, Appl. Catal. B: Environ. 29 (2001) 47.
[20] X. Wang, H.Y. Ch, W.M.H. Sachtler, Appl. Catal. B: Environ. 26 (2000) L227.
[21] R.A. Schoonheydt, L.J. Vandamme, P.A. Jacob, J.B. Vyherhoeven, J. Catal. 43 (1976) 292.
[22] J.Y. Yan, H.H. Kung, W.M.H. Sachtler, M.C. Kung, J. Catal. 175 (1998) 294.
[23] A. Boix, E. Miró, E.A. Lombardo, unpublished results.